Werk

Jahr: 1986
Kollektion: fid.geo
Signatur: 8 Z NAT 2148:59
Digitalisiert: Niedersächsische Staats- und Universitätsbibliothek Göttingen
Werk Id: PPN1015067948_0059
PURL: http://resolver.sub.uni-goettingen.de/purl?PPN1015067948_0059

LOG Id: LOG_0019
LOG Titel: Modelling active audio-magnetotelluric data
LOG Typ: article

Übergeordnetes Werk

Werk Id: PPN1015067948
PURL: http://resolver.sub.uni-goettingen.de/purl?PPN1015067948
OPAC: http://opac.sub.uni-goettingen.de/DB=1/PPN?PPN=1015067948

Contact

Niedersächsische Staats- und Universitätsbibliothek Göttingen
Georg-August-Universität Göttingen
Platz der Göttinger Sieben 1
37073 Göttingen
Germany
Email: gdz@sub.uni-goettingen.de

J Geophys (1986) 59:49–55

Journal of Geophysics

Modelling active audio-magnetotelluric data

G. Fischer and P.-A. Schnegg
Observatoire Cantonal, CH-2000 Neuchâtel, Switzerland

Abstract. A major improvement in the new pulsed AMT method recently proposed by the authors has been achieved by modelling the field data with the analytic response of layered structures to point-source excitations. The pulsed field data can be modelled quickly to yield the best-fitting one-dimensional model. Small departures from one-dimensionality often seem to manifest themselves as a rotation of the transmitted fields through a vertical axis. This rotation can also be modelled and leads to a significant improvement of the fit. A trade-off analysis of the model parameters shows that these are well constrained in the practical example considered. The correct number of layers with which to model the data can also be derived with confidence.

Key words: Active audiomagnetotellurics – Modelling active magnetotelluric data

Introduction

Electromagnetic sounding methods using artificial or controlled signal sources are gaining in popularity, perhaps as a consequence of the ever-increasing level of perturbations caused by human activity. Ward (1983) has reviewed some of these methods and their application to deep exploration. Recent examples of the use of controlled sources in magnetotellurics (MT) or audiomagnetotellurics (AMT) have been described by Sandberg and Hohmann (1982), Otten and Musmann (1983), Adam et al. (1983), Szarka (1983) and Heikka et al. (1984).

Schnegg and Fischer (1984) have recently set up a method with which it is possible to perform a natural-source and a controlled-source AMT sounding in quick succession with the same equipment. The implementation of their method to one-dimensional (1D) or layered structures was based on the following observation. If, at constant period T, the logarithm of the apparent resistivity, $\log \rho_a(r, T)$, and the phase, $\varphi(r, T)$, are plotted against the inverse distance, $1/r$, to a grounded dipole source (cf. Fig. 1), a linear behaviour is usually observed over a broad range of large source-receiver separations r. As the distance r is allowed to become larger still, the signal strength becomes weaker and the data scatter increases. It was tempting, therefore, to assume that the $1/r$ trend was the limiting asymptotic behaviour of $\log \rho_a$ and φ when r becomes very large. This was questioned (Musmann, personal communication), however, and indeed a number of analytical computations of the response of 1D structures to grounded dipole excitation (Sunde, 1949; Goldstein and Strangway, 1975; Kauahikaua, 1978) show that the behaviour of $\log \rho_a(r, T)$ and $\varphi(r, T)$ is in fact more complicated than Schnegg and Fischer (1984) had assumed. Figure 2, which illustrates this point, was computed with an analytical program kindly supplied by Dr. Weidelt (personal communication). This figure confirms both the more complicated behaviour at large distances and the apparently linear trend observed experimentally over a wide range of inverse distances. It also shows, however, that extrapolating the linear portion toward the $1/r=0$ limit does not yield the correct far-field or MT values.

Because of limitations in the signal power available, the far-field condition between source and receiver can often not be achieved. We have thus asked ourselves whether it was possible, under the assumption of one-dimensionality, to model the near-field data with Weidelt's forward analytical program.

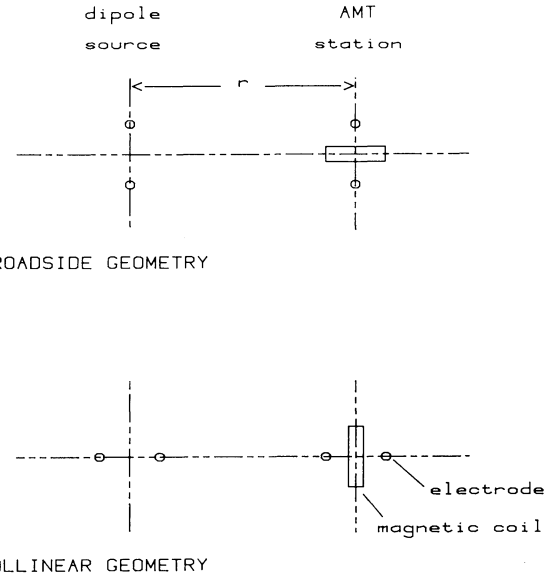

Fig. 1. Sketch of the configurations for broadside and collinear soundings in controlled-source AMT

Offprint requests to: Gaston Fischer

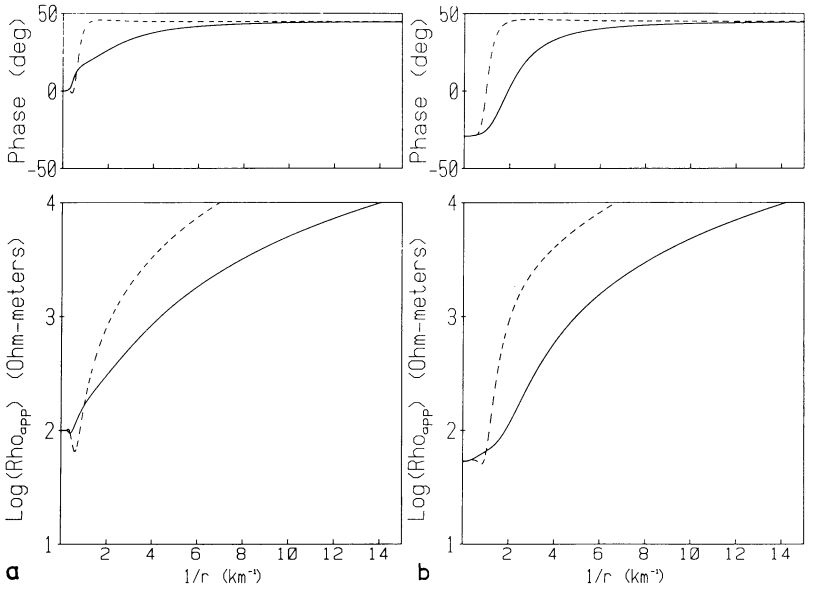

Fig. 2. a Logarithm of apparent resistivity and phase versus the inverse distance from a 100-Hz ac grounded dipole source at the surface of a uniform half-space of 100-Ωm resistivity. The phase plotted is 45° minus the lag of the electric versus the magnetic fields (cf. Fischer et al., 1981). The *full curve* refers to broadside excitation, the *dashed curve* belongs to the collinear geometry (cf. Fig. 1). **b** Plot similar to Fig. 2*a*, but for a half-space with 1-Ωm resistivity, covered with a 250-m overburden of 100 Ωm

Modelling near-field MT data

The past few years have witnessed great improvements in the methods of modelling natural (i.e. far-field) one-dimensional MT and AMT data. Among these many new schemes, Fischer and Le Quang (1981, 1982) have proposed an efficient search routine to find the layered model which gives the best fit, in the least squares sense, to a given field data set. This search routine has also been used successfully to model other kinds of data, like Schlumberger or Wenner apparent resistivities. It also proved very well suited to model near-field MT or AMT data, as can be seen in Fig. 3. The data in this figure were obtained over a dried-up marsh in the Swiss Molasse Basin. The site is level with near perfect horizontal layering. The top layers consist of a few metres of peat and a succession of recent Quaternary sediments, the total thickness of which is not known exactly at the BELE sounding site but probably does not exceed 50–100 m. This is followed by a series of sandstones typical of the Swiss Molasse Basin, down to a depth of the order of 500–1000 m (Axelrod, 1978; Schlanke et al., 1978) where the transition to the much more resistive Jura limestones takes place, with resistivities in the range 180–1000 Ωm.

At the site of Fig. 3, data have been gathered with the source placed at 14 different distances from 200 to 1659 m. At the greatest separation the data scatter is somewhat larger than that visible in Fig. 3. As the distance of injection is reduced the scatter decreases, but plots of log ρ_a and φ versus the period T also become more and more featureless. It seems preferable, therefore, to model intermediate distances in the range 500–1000 m for our AMT periods and the rather low resistivities of the BELE site.

A rather striking feature in Fig. 3 is the greater variation with distance of the measured data when compared to the computed data. This feature is not peculiar to the BELE site, but has been observed repeatedly at other sites, all of which could be considered, from independent geological evidence, to be fairly 1D. It is worth stressing, as Fig. 3 clearly shows, that this is a systematic effect, much larger than – and obviously distinct from – the intrinsic data scatter, and it therefore contributes significantly to the rather large standard deviation E.

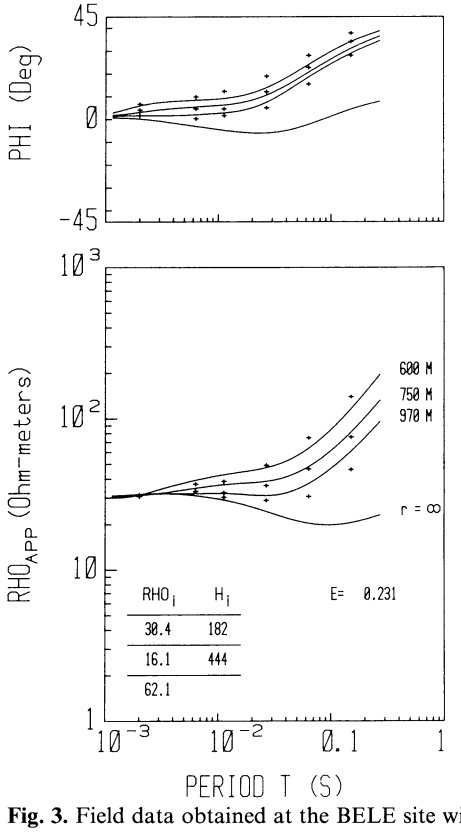

Fig. 3. Field data obtained at the BELE site with pulsed excitation at distances of 970, 750 and 600 m in the broadside configuration (cf. Fig. 1). These data have been modelled with a three-layer structure whose best-fitting parameters are shown in the inset, together with the standard deviation E between computed curve and measured data. Also shown is the computed AMT curve ($r = \infty$) for the model found. The standard deviation E is computed according to Fischer et al. (1981), without weighting the data. To reduce computing time, the data from six periods only have been modelled

In attempting to identify the cause of this stronger dependence of the field data on the distance separating current source and receiver station our first idea was to check whether it could be due to the presence of a highly conduct-

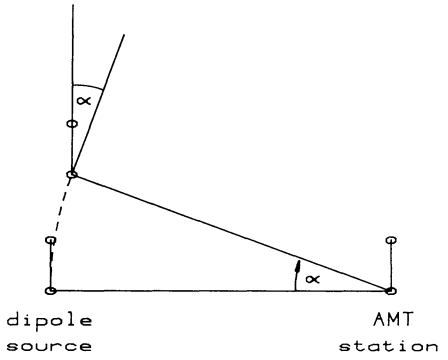

Fig. 4. Geometrical configuration for broadside injection: the source and receiver electrode pairs are placed at right angles to the line joining the two sites (cf. Fig. 1). If the field at the receiving station appears to have been rotated around a vertical axis by an angle α, this is equivalent to assuming that the transmitter has been moved without rotation and is seen under an azimuth α with respect to the original direction

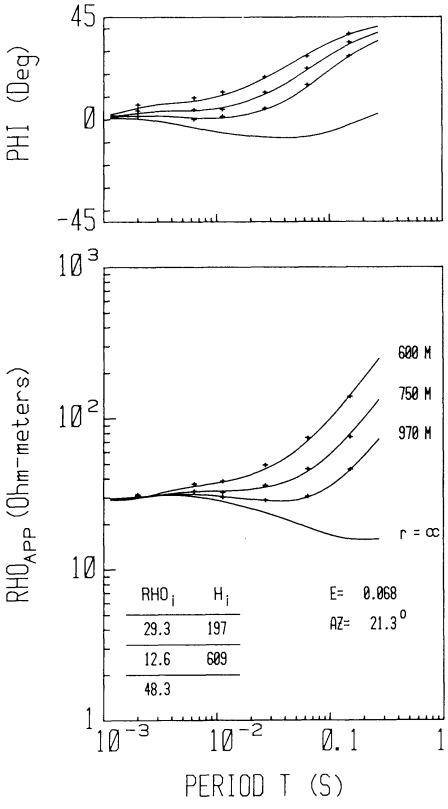

Fig. 5. Plot similar to Fig. 3, but assuming that the fields at the receiving station have been rotated through an angle $\alpha = 21.3°$. This angle corresponds to the most suitable combination of broadside (cos α) and collinear (sin α) geometries

ing thin overburden, but this proved fruitless. We then remembered, as Fig. 2 shows, that the collinear geometry yields data which vary more rapidly with distance than broadside data. Although the data of Fig. 3 refer to the broadside geometry (cf. Fig. 1), with current injection and receiving electrodes both perpendicular to the line joining the two sites, we decided to treat the received signal as if it were a combination of broadside and collinear fields. In other words, we considered the fields recorded at the receiving site as having been rotated through an angle α around a vertical axis. Looking at Fig. 4, this is equivalent to the assumption that the point-source has been moved without rotation and is now seen from the receiving station under an azimuth α with respect to the original source-receiver direction. Our minimizing routine is therefore instructed to select not only the best-fitting model, but also the most appropriate azimuth. We see in Fig. 5 that this procedure is very effective: it brings the standard deviation back to a value well below $E = 0.1$, while requiring only a modest rotation of $\alpha = 21.3°$. The structural model found remains fairly close to the one achieving the best possible fit without the rotation.

We should also like to stress that phase and apparent resistivity appear to contribute equally to the model determination. Our graphs, as for example Fig. 5, are constructed with ordinate scales which give log ρ_a and φ the same sensitivity (cf. Fischer et al., 1981). With such representations one generally observes a larger scatter of the MT or AMT phase than of the corresponding log ρ_a. With our pulsed technique we are able to secure phase data which seem much less scattered, and it is gratifying to see that our modelling scheme makes full use of these improved phase data.

Justification of a non-vanishing azimuth

As we said above, the respective configurations of the grounded dipole source and of the receiving electrodes and magnetic sensing coil refer to the broadside geometry as defined in Fig. 1. If the structure were perfectly one-dimensional, the data could be expected to yield a strictly broadside response. Several factors, however, are likely to distort the transmitted field which, at the receiving station, would then appear as a mixture of broadside and collinear components: (1) small misalignment errors at the transmitting and receiving stations are unavoidable, amounting to perhaps a degree or two; (2) naturally occurring structures are never ideally 1D and both lateral variations of geometry as well as of resistivity, even in the same formation, must be expected to lead to rotations of the field; (3) another frequent departure from ideal 1D conditions lies in the topography which is seldom perfectly level; (4) the field may also suffer distortions and will therefore appear as having been rotated, because of artificial sub-surface metal structures like drainage pipes and other conduits.

As was said before, the data displayed in Fig. 5 were obtained at the surface of a dried-up marsh. This site is therefore quite level, but the sounding area is crossed by a number of drainage channels and the sediments at depth cannot be taken as forming a perfect horizontal layering (Axelrod, 1978). After modelling the entire data set with a single model structure and a single azimuth α, the fit cannot be improved much if a different azimuth is allowed for each distance r. A different azimuth $\alpha(r)$ for different injection distances r must be expected, however, as the four factors listed above will contribute differently when the injection site is moved. As an example of this we give, in Table 1, the azimuths obtained when we model data sets arising from groups of three injection distances, where these distances are systematically decreased. We note in this table that the azimuth appears to become smaller when the sources move closer. This is what one would expect from

Table 1. Model parameters and azimuths obtained at the BELE site when the signal sources are moved closer to the receiving station

Injection distances [m]	ρ_1 [Ωm]	h_1 [m]	ρ_2 [Ωm]	h_2 [m]	ρ_3 [Ωm]	E	Azimuth
970 750 600	29.3	197	12.6	609	48.3	0.0681	21.3°
750 600 500	29.6	201	13.2	654	58.3	0.0772	18.5°
600 500 429	29.6	199	14.0	835	35.9	0.0787	17.2°
500 429 375	30.4	188	14.9	844	39.7	0.0883	16.0°
429 375 333	30.8	177	16.2	882	35.9	0.0995	16.5°

the major causes of field rotation we have envisaged. Table 1 also shows that the five model parameters are quite stable with respect to the varying distance of the source. As we have said before, however, the response curves are less well featured when the sources move closer to the receiver, and modelling then loses resolution.

The results displayed in Table 1 also suggest that it will generally suffice to acquire data with the dipole source placed at two or three different locations, with distances approximately in the range of one half to one skin-depth for the longer periods recorded. For the BELE site the MT apparent resistivity is about 20 Ωm (cf. Fig. 5) and, with long periods of around 0.1 s, we have an apparent skin-depth of about 700 m in agreement with our observation that injection distances in the range from 500 to 1000 m seemed most appropriate for this site. Distances larger than these would of course also be suitable, but they would require a more powerful signal source than ours.

Parameter trade-off

When geophysical data are modelled it is crucial to ask whether a given sounding method leads to models which are well constrained or whether the model parameters one derives are susceptible of large variations, i.e. are poorly resolved. Because the new pulsed AMT technique leads to data which are far less scattered than those of traditional AMT, it is of interest to determine the range of definition of the derived model parameters. As we have shown elsewhere (Fischer and Le Quang, 1982), this can best be done by way of a parameter trade-off analysis in which one looks for the family of models whose standard deviation E remains within 10% of the minimum value E_o. Taking the data of Fig. 5 as an example, with $E_o = 0.068$, each of the model parameters in turn is varied systematically to larger or smaller values. Under the constraint of the imposed variation *all the other parameters are adjusted to minimize E.* The set of limiting parameters are obtained when $E = 1.1\ E_o$. These limiting parameters can be expressed in terms of those of the best-fitting model and are represented in the form of a parameter trade-off diagram as shown in Fig. 6. In this diagram the trade-off limits are given by the full lines. The dashed lines define the narrower ranges where E reaches $1.1\ E_o$ when a given model parameter is varied *without adjusting* the other parameters to minimize E.

What Fig. 6 shows is that, with the exception of the basement resistivity ρ_3, all the model parameters are extremely well constrained: ρ_1, h_1, and ρ_2 have variation ranges of less than 10% around their best-fitting values; for h_2 the limits are −17% and +28%; and while there is a very large upper bound at 3000 Ωm for ρ_3, its lower bound at 23 Ωm is only a factor of two below the best-fitting value of 48.3 Ωm. The trade-off analysis also yields a range of permitted azimuths α. This range, from $\alpha = 17.2°$

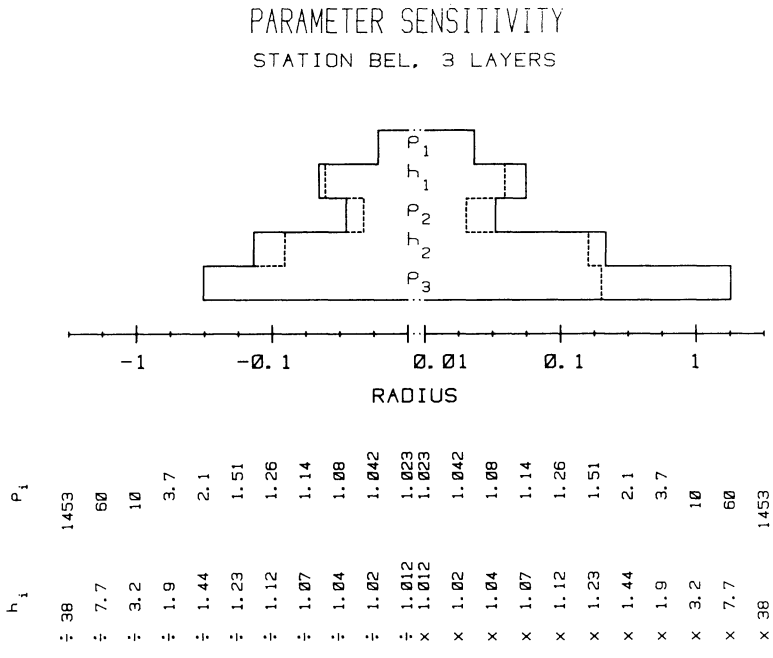

Fig. 6. Trade-off diagram for the data and model of Fig. 5 (cf. Fischer and Le Quang, 1982). The radii refer to distances in the space of model parameters. The scales are logarithmic and normalized to the parameters of the best-fitting model. The diagram gives the parameter range within which the standard deviation E exceeds the minimum E_o of the best model by less than 10%. Note the different scales for ρ_i/ρ_{i0} and for h_i/h_{i0}. As an example, h_2 can be varied between $h_{20}/1.10$ and $1.20\ h_{20}$ without changing the other parameters (*dashed limits*), and between $h_{20}/1.17$ and $1.28\ h_{20}$ if the other parameters are adjusted to keep E minimal under the imposed variation of h_2 (*solid limits*). The solid limits thus give the extreme excursions of the parameters within which it is possible to achieve $E \leq 1.10\ E_o$. This same procedure yields a maximum range of 17.2°–24.0° for the azimuth α

to $\alpha = 24.0°$, is very narrow and therefore rather supports the assumption that the fields at the receiving station have undergone a small rotation around a vertical axis.

It is of interest to compare the trade-off diagram of Fig. 6 with similar diagrams for typical MT data (cf. Fig. 4 of Fischer and Le Quang, 1982). Quite clearly the new pulsed AMT method leads to model parameters which are far more precisely defined. In part this is of course a consequence of the much smaller scatter of the data, possible with a controlled-source technique, but it is probably also an inherent property of this particular method based on a grounded dipole source.

How many layers are resolved?

The trade-off diagram of Fig. 6 makes it clear that the resistivity ρ_3 of the lowermost layer is poorly resolved. It may therefore seem questionable whether the data support a structure with three layers, or whether a model with only two layers would not explain them equally well. There is more reason to ask such a question with the controlled-source method than with natural MT or AMT, because the shape of the response curves does not immediately suggest a minimum number of necessary layers. This is true equally for the shape of the responses as function of distance (cf. Fig. 2a and b) and for their shape when plotted versus the period (cf. Fig. 5). The natural AMT curves in Fig. 5, labelled $r = \infty$, are quite clearly three-layer curves. That this is not self-evident for the controlled-source curves can be seen in Fig. 7, where the analytical response has been plotted for a two-layer model which turns gradually into a three-layer model. Again the far-field curves ($r = \infty$) at once suggest the correct number of layers, whereas nothing similar can be deduced from the near-field curves.

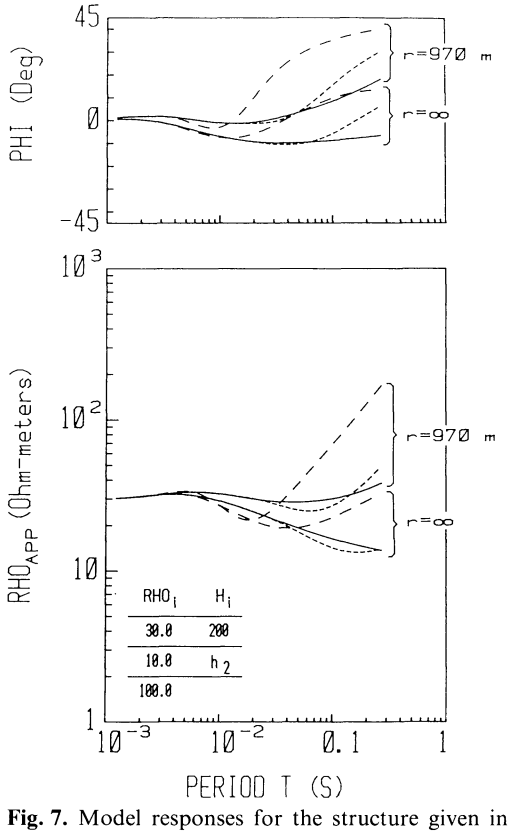

Fig. 7. Model responses for the structure given in the inset. The *full lines* correspond to $h_2 = \infty$, i.e. a structure with only two layers. The *dotted curves* refer to $h_2 = 500$ m and the *dashed curves* to $h_2 = 150$ m. The sets of three curves each correspond to source-receiver distances of 970 m and infinity. This graph illustrates the difficulty of deciding visually whether a given response is caused by structures with two or three layers

Table 2. Modelling the field data with a varying number of layers. These data demonstrate that three layers are appropriate. With four layers the standard deviation E decreases by 0.5%; with only two layers it increases by 42%

n	ρ_1 [Ωm]	h_1 [m]	ρ_2 [Ωm]	h_2 [m]	ρ_3 [Ωm]	h_3 [m]	ρ_4 [Ωm]	Azimuth [degrees]	E
1	19.8	∞						1.8	0.5238
2	29.7	187	13.9	∞				20.6	0.0964
3	29.3	197	12.6	609	48.3	∞		21.3	0.0681
4	29.4	195	12.9	487	18.4	345	57.5	21.4	0.0677

In spite of the impossibility of establishing a realistic estimation of the correct number of layers merely by looking at the observed response curves, other arguments can be called upon to derive this number with confidence. We propose to show with the example of Fig. 5 that these data indeed give evidence in favour of a three-layer structure.

While the trade-off diagram of Fig. 6 does show ρ_3 to be poorly determined, it gives all the other model parameters as very well resolved; in particular h_2 and $h_1 + h_2$, i.e. the depth to the basement layer. An even more powerful argument is obtained when we attempt to model the field data with different numbers of layers, as seen in Table 2. The standard deviation E between field and model data can be reduced to $E = 0.0681$ if a three-layer model is postulated. This value can almost not be reduced further with a four-layer model, but it jumps by 42% to $E = 0.0964$ when modelling with only two layers. Obviously three layers is the correct number to postulate.

Comparison of natural and controlled source AMT

In Fig. 8 we have plotted the results of a natural AMT sounding at the BELE site, together with the response curve from the best-fitting model yielded by the controlled-source sounding. Also plotted in Fig. 8 are the data resulting from the linear extrapolation against the inverse distance described previously (Schnegg and Fischer, 1984). As already noted, the latter data are systematically too low, both as regards the apparent resistivity and the phase. The comparison of the natural- and controlled-source responses is of more interest. There is strong disagreement between the two responses at the longer periods. This is not surprising since it is precisely at the long periods that artificial perturbations propagate furthest. At periods shorter than about 0.1 s, the skin-depth and thus the extent of the perturbations have decreased and the two sounding methods yield concordant results. At the very shortest periods there is a hint that the natural sounding data again deviate from the controlled-source response. We believe that this is of instrumental origin: at periods below 2 ms the signal to noise ratio of our system begins to deteriorate and generally the amplitude of the natural signals becomes weaker toward 1 or 2 kHz.

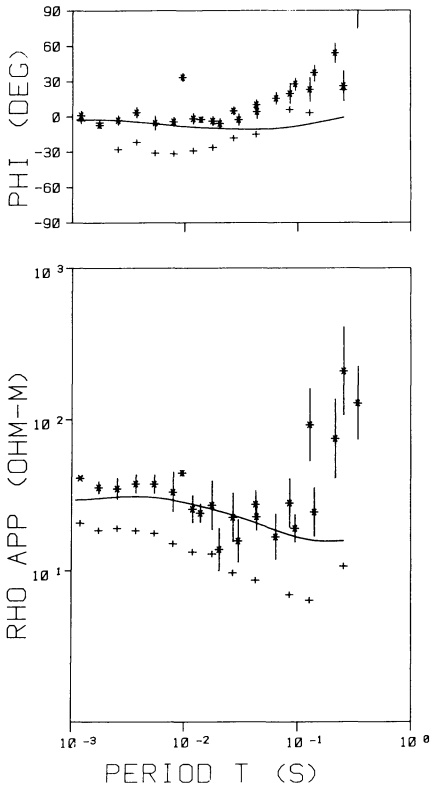

Fig. 8. Comparison of natural source AMT data (*stars*) with the response of the model derived from the active-source AMT (*smooth curve*) at the BELE site. The diagram also shows the results obtained by the linear extrapolation of $\log \rho_a$ and φ against $1/r$ (*crosses*) originally proposed by the authors (Schnegg and Fischer, 1984)

We return now to the family of models required by the controlled-source sounding and specified jointly by the best-fitting model given in Fig. 5 and the extremal model parameters according to the trade-off diagram of Fig. 6. It is of course meaningless to attribute great significance to the parameters of the top layer. With a shortest period of about 1.5 ms and a 30-Ωm resistivity, the skin-depth is about 106 m; variation within the thin and highly conducting Quaternary formations can, therefore, not be resolved. All that can be said is that the upper 100–200 m behave as if they had a conductance of about $h_1/\rho_1 = 6.7$ S, but these top formations certainly comprise several separate layers of different resistivities. Note that the trade-off diagram gives ρ_1 and h_1 with uncertainties of less than $\pm 10\%$. The second layer is the only one which is well resolved: $11.8 \leq \rho_2 \leq 13.6$ Ωm and $520 \leq h_2 \leq 780$ m. It follows, therefore, that the depth to the limestones, i.e. $h_1 + h_2$, is comprised between about 610 and 990 m, in perfect accord with the other geophysical and geological knowledge available for this site (Axelrod, 1978; Schlanke et al., 1978). As was said before, with a range of 23–3000 Ωm, the limestone resistivity is the least well resolved. Its true value in this area is in the range 180–1000 Ωm.

Conclusion

The new pulsed AMT method proposed by Schnegg and Fischer (1984) is somewhat more complicated than these authors had assumed on the basis of their experimental observations. However, the field data which are obtained with the new technique are clearly far more reproducible and less scattered than natural AMT data. It was therefore worth investigating whether the data obtained by this new method could be modelled with a one-dimensional algorithm. We were able to achieve this with the same search routine used previously to model natural MT or AMT data (Fischer and Le Quang, 1981). Our artificial AMT technique thus remains an efficient new electromagnetic sounding tool.

The detailed study of a set of field data suggested that the various departures from ideal one-dimensionality, like lateral changes of the structure or topographical accidents, seem to lead to small rotations of the polarization plane of the field. This can easily be taken care of by determining not only the model that fits the field data best, but also the most appropriate azimuth.

The MT or AMT responses of layered structures to natural, or far-field, excitations give very explicit visual indications about the minimum number of layers necessary to model measured data. With our artificial near-field data this information is less direct, but it can be derived with equal confidence by way of a trade-off analysis and by modelling with fewer or more layers. The trade-off analysis indicates that the model parameters derived are generally well resolved.

The new method was applied to the determination of the depth to the limestones at a site in the Swiss Molasse Basin. It gave this depth as 800 ± 190 m at that particular site, in perfect accord with independent Schlumberger soundings (Axelrood, 1978).

Acknowledgements. Quite obviously we are particularly indebted to Dr. P. Weidelt for the very efficient computer programs he kindly made available to us. Without these programs this paper could never have been written. Financial assistance was gratefully received from the Swiss National Science Foundation and from the Geophysical Commission of the Academy of Natural Sciences.

References

Adam, A., Szarka, L., Varga, M.: Physical and mathematical modelling of crustal conductivity anomalies in the Pannonian Basin. Acta Geodaet., Geophys. et Montanist. Hung. **18**, 467–488, 1983

Axelrod, A.: Contribution à l'étude géophysique de la région des Lacs de Neuchâtel, Bienne et Morat. Thèse de doctorat présentée à la Faculté des Sciences (Institut de Géophysique) de l'Université de Lausanne, 1978

Fischer, G., Le Quang, B.V.: Topography and minimization of the standard deviation in one-dimensional magnetotelluric modelling. Geophys. J.R. Astron. Soc. **67**, 279–292, 1981

Fischer, G., Le Quang, B.V.: Parameter trade-off in one-dimensional magnetotelluric modelling. J. Geophys. **51**, 206–215, 1982

Fischer, G., Schnegg, P.-A., Peguiron, M., Le Quang, B.V.: An analytic one-dimensional magnetotelluric inversion scheme. Geophys. J.R. Astron. Soc. **67**, 257–278, 1981

Goldstein, M.A., Strangway, D.W.: Audio-frequency magnetotellurics with a grounded electric dipole source. Geophysics **40**, 669–683, 1975

Heikka, J., Zhamaletdinov, A.A., Hjelt, S.E., Demidova, T.A., Velikhov, Ye. P.: Preliminary results of MDH test registrations in northern Finland. J. Geophys. **55**, 199–202, 1984

Kauahikaua, J.: Electromagnetic fields about a horizontal electric wire source of arbitrary length. Geophysics **43**, 1019–1022, 1978

Otten, J., Musmann, G.: Aktive Audiomagnetotellurik bei Travale. Protokoll Elektromagnetische Tiefenforschung, Neustadt a.W., pp. 183–188, 1982. See also Musmann, G., Otten, J.: Active audiomagnetotelluric application in geothermal areas. Abstract I3.18/IAGA XVIII General Assembly, Hamburg, August 15–27, 1983

Sandberg, S.K., Hohmann, G.W.: Controlled-source audiomagnetotellurics in geothermal exploration. Geophysics **47**, 100–116, 1982

Schlanke, S., Hauber, L., Büchi, U.: Lithographie und Sedimentpetrographie der Molasse in den Bohrungen Tschugg 1 und Ruppoldsried 1 (Berner Seeland). Eclogae Geologicae Helvetiae **71**, 409–425, 1978

Schnegg, P.-A., Fischer, G.: A new pulsed audiomagnetotelluric technique. J. Geophys. **55**, 191–198, 1984

Sunde, E.D.: Earth conduction effects in transmission systems. London: D. Van Nostrand Co. Inc. 1949

Szarka, L.: Exploration of high resistivity basement using electrical and magnetic fields of quasi-static point sources. Geophys. Prosp. **31**, 829–839, 1983

Ward, S.H.: Controlled source electrical methods for deep exploration. Geophys. Surv. **6**, 137–152, 1983

Received May 10, 1985; Revised version September 2, 1985
Accepted September 6, 1985